



LAWRENCE  
LIVERMORE  
NATIONAL  
LABORATORY

# A Compact UV Timing Fiducial System for use with x-Ray Streak Cameras at NIF

D. Homoelle, M. Bowers, D. Browning, S. Burns, B. Golick, G. Erbert, J. Haley, T. McCarville, E. Padilla, N. Palmer, B. Perfect, L. Pelz, T. Spinka, A. Throop, J. N. Wong

August 13, 2012

A Compact UV Timing Fiducial System for Use with x-Ray Streak Cameras at NIF  
San Diego, CA, United States  
August 12, 2012 through August 16, 2012

## **Disclaimer**

---

This document was prepared as an account of work sponsored by an agency of the United States government. Neither the United States government nor Lawrence Livermore National Security, LLC, nor any of their employees makes any warranty, expressed or implied, or assumes any legal liability or responsibility for the accuracy, completeness, or usefulness of any information, apparatus, product, or process disclosed, or represents that its use would not infringe privately owned rights. Reference herein to any specific commercial product, process, or service by trade name, trademark, manufacturer, or otherwise does not necessarily constitute or imply its endorsement, recommendation, or favoring by the United States government or Lawrence Livermore National Security, LLC. The views and opinions of authors expressed herein do not necessarily state or reflect those of the United States government or Lawrence Livermore National Security, LLC, and shall not be used for advertising or product endorsement purposes.

# A compact UV timing fiducial system for use with x-ray streak cameras at NIF

Doug Homoelle, Mark Bowers, Don Browning, Scott Burns, Gaylen Erbert, Brad Golick, Jim Haley, Tom McCarville, Yekaterina Opachich, Ernesto Padilla, Nathan Palmer, Brad Perfect, Larry Pelz, Tom Spinka, Alan Throop, J. Nan Wong.

Lawrence Livermore National Laboratory, 7000 East Ave., Livermore, USA

## ABSTRACT

We present the design of a compact UV (263-nm) timing fiducial system for use with x-ray streak cameras at the National Ignition Facility (NIF). The design consists of remote fiber amplification of an infrared 1053-nm ( $1\omega$ ) seed, a free-space optical path that has two stages of frequency conversion from  $1\omega$  to the fourth harmonic ( $4\omega$ ), and fiber delivery of the  $4\omega$  signal via output fiber for use with an x-ray streak camera. This is all contained within an airbox that can reside in a vacuum. The  $1\omega$  seed and the pump light for the fiber amplifier is delivered to the airbox via optical fiber ( $\sim 100$  meters) from a location in the NIF that is shielded from neutron radiation generated from imploding targets during system shots. When complete, the system will be able to provide timing fiducials to multiple x-ray streak cameras on the same system shot. We will present data that demonstrates end-to-end system performance.\*

**Keywords:** National Ignition Facility, Timing Fiducial, X-Ray Streak Camera, Diagnostics, Fiber Laser Amplifier, Fourth-harmonic generation

## 1. INTRODUCTION

X-ray streak cameras are critical diagnostics for the National Ignition Campaign (NIC) that is currently underway at the National Ignition Facility (NIF). These streak cameras<sup>1</sup> will be used to measure implosion velocity and remaining ablator mass versus time on converging ablator experiments with the Diagnostic Instrument Manipulator (DIM) Imaging Streak Camera (DISC).<sup>2</sup> The Streaked Polar Instrumentation for Diagnosing Energetic Radiation (SPIDER) diagnostic uses an X-ray streak camera to measure x-ray burn history on higher-yield shots.<sup>3</sup> Because streak cameras are nonlinear in time and have a certain amount of timing jitter an accurate calibration of the time axis on the streak camera data in these experiments is necessary to meet the required timing accuracy of the experiment: 2-ps uncertainty over a 300-ps time window.

Multiple timing fiducial combs for visible streak cameras are already in use on NIF,<sup>4</sup> but their wavelengths of operation are typically in the visible or infrared range. The photocathodes for the X-ray streak cameras are not sensitive to this wavelength, *i.e.* infrared and visible light do not generate photoelectrons with materials typically used for x-ray streak cameras. X-ray photocathode materials on NIF diagnostics are typically gold (Au) or cesium iodide (CsI). However, photoelectrons can be generated with these materials as the wavelength reaches the ultraviolet range. Therefore, a proposal was made to generate a comb of ultraviolet pulses to serve as a timing fiducial for the X-ray streak cameras by frequency quadrupling the fundamental wavelength used at NIF, 1053-nm ( $1\omega$ ), to generate the 4th harmonic ( $4\omega$ ). This diagnostic has been named the  $4\omega$ -fiducial system, or  $4\omega$ -fidu for short.

An initial system was designed and built by the Laboratory for Laser Energetics (LLE) in which the fiducial comb was generated by regeneratively amplifying a  $1\omega$  pulse that was frequency doubled to the second harmonic ( $2\omega$ ) and then frequency doubled again to generate the fourth harmonic.<sup>5</sup> This system produced more than adequate fourth-harmonic energy, up to 100's of microjoules per pulse, which was then coupled into a 25-meter large-core (600- $\mu\text{m}$ ) UV fiber and could be delivered to the DISC in the target chamber. The 25-meter fiber attenuated the signal at a rate of 0.5 dB/m and also broadened the pulse in time due to modal dispersion from

---

\*Lawrence Livermore National Laboratory is operated by Lawrence Livermore National Security, LLC, for the U.S. Department of Energy, National Nuclear Security Administration under Contract DE-AC52-07NA27344.

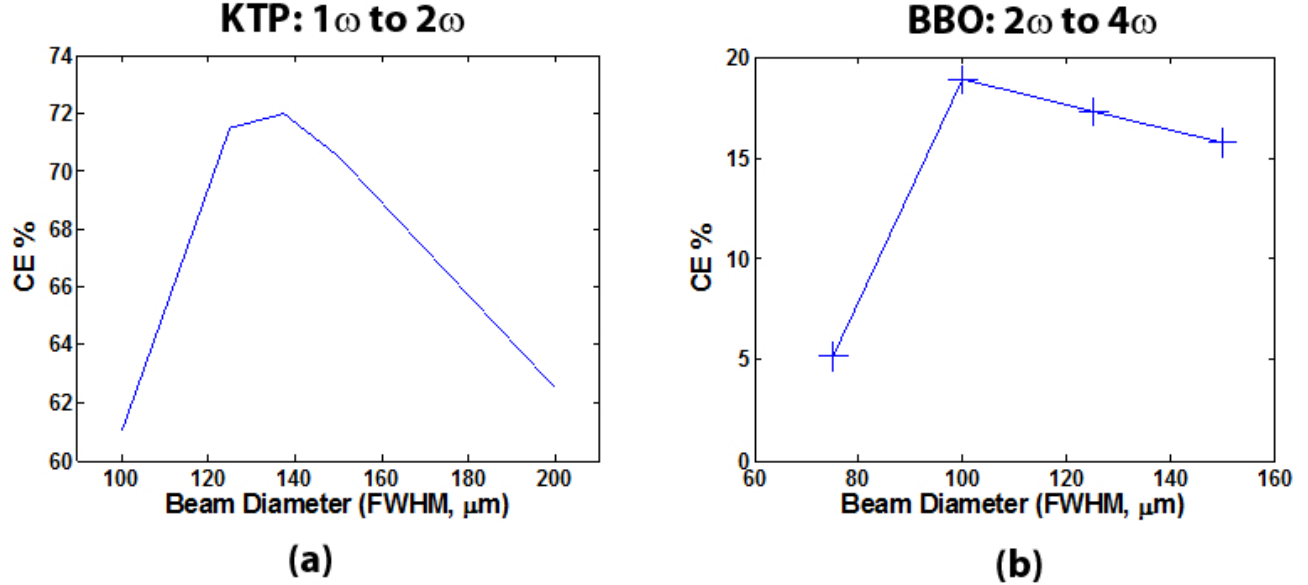


Figure 1. Conversion efficiency as a function beam diameter in 15-mm long KTP crystal (a) and 15-mm long BBO crystal (b) as calculated by SNLO. The input energy for the KTP crystal was  $2\mu\text{J}$  and the pulse width was 90 ps. The input energy for the BBO calculation was  $1.4\mu\text{J}$  and the pulse width was 64 ps.

the many modes that propagate in a  $600\text{-}\mu\text{m}$ -core fiber, but these effects were sufficiently benign that the system met all energy and timing requirements for the  $4\omega$ -fiducial system. However, because of concerns about neutron damage to some of the electronics in the regen laser due to its close proximity to the target chamber, and because of a desire to deliver  $4\omega$  fiducial pulses to multiple locations on a single shot, a new system design was required that could accommodate these new requirements. A description of the design and performance of such a system is the subject of this paper.

## 2. DESIGN

In order to move the sensitive electronics outside of the target chamber to protect them from neutron damage, a delivery fiber of  $\sim 100$  meters is necessary. Sending the  $4\omega$  signal directly from the regen laser system was not an option because the signal would be too attenuated over such a long distance, so it was decided that either  $1\omega$  or  $2\omega$  must be delivered to a frequency-conversion stage that was local to the actual streak camera. However, in order to deliver  $1\omega$  or  $2\omega$  pulses with sufficient energy for frequency conversion the Raman threshold of a typical single mode fiber would be greatly exceeded. We considered using a large-core fiber at these wavelengths to reduce the Raman threshold (which is sensitive to intensity) but the mode quality at the output of a fiber with a sufficiently large core was so poor that it would not be possible to focus the output tightly enough to generate a sufficient frequency conversion. We therefore decided to deliver only the  $1\omega$  seed and the pump light necessary to amplify the seed to the remote location near the streak camera, and do both the amplification and frequency conversion in the remote location.

In order to keep the system compact and minimize its complexity, we decided to use a fiber amplifier system in the remote location. Initial  $4\omega$  experience with the LLE laser suggested  $100\text{nJ/pulse}$  of  $4\omega$  energy was sufficient to serve as a fiducial on the streak camera. With this goal in mind, we used SNLO software<sup>6</sup> to explore different  $1\omega$  pulse energies and beamsizes, as well as different nonlinear crystals parameters, to determine the required  $1\omega$  energy to achieve the necessary  $4\omega$  signal. Figure 1(a) shows the conversion efficiency of a 90-ps,  $2\text{-}\mu\text{J}$   $1\omega$  pulse to the second harmonic as a function of beam diameter through 15-mm of KTP crystal. This model predicts 70% conversion efficiency from  $1\omega$  to  $2\omega$  under these conditions. Figure 1(b) shows the conversion efficiency of a  $\sim 63$ -ps,  $1.4\text{-}\mu\text{J}$  pulse to  $4\omega$  as a function of beam diameter through 15mm of BBO crystal. The shorter pulse

width for the  $2\omega$  signal reflects the reduction in pulse width that occurs due to the intensity dependent nature of the frequency conversion process and the fact that we have an approximately Gaussian pulse in time. The model predicts a maximum conversion efficiency of 19% from  $2\omega$  to  $4\omega$  under these conditions, which would result in  $>250\text{nJ}$  of  $4\omega$  light for  $2\text{-}\mu\text{J}$  of  $1\omega$  input energy. In practice we have not been able to achieve the calculated  $1\omega$ -to- $2\omega$  conversion efficiency for reasons that will be discussed below.

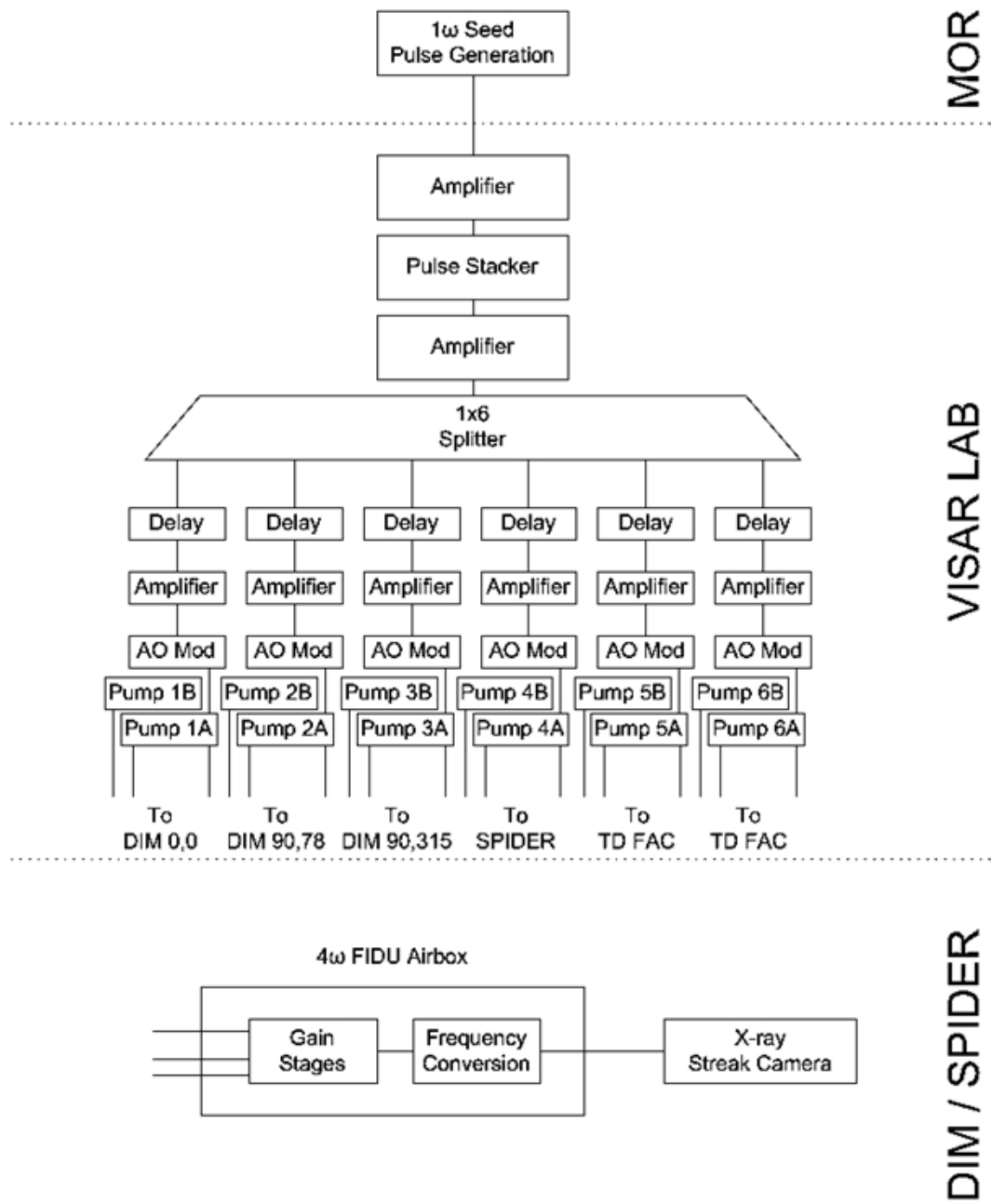
A major concern when dealing with these energy levels in a fiber amplifier is damage to the fiber. The damage threshold for fused silica at  $1053\text{ nm}$  for a  $90\text{-ps}$  pulse is  $10\text{ J/cm}^2$ .<sup>7</sup> For a fiber with a  $6\text{-}\mu\text{m}$  mode-field diameter, this corresponds to a pulse energy of  $\sim 2.8\mu\text{J}$ . The  $2\mu\text{J/pulse}$  requirement derived above placed us just below this damage threshold. We therefore had to be very careful to not exceed this threshold with any of the six pulses in the pulse train, and also to keep the fiber tip surface at the end of the fiber very clean.

The seed pulse for the  $4\omega$  system is generated in the master oscillator room (MOR) at NIF.<sup>8</sup> This seed is delivered to the VISAR room at NIF which is located just outside the target chamber. A rack-mounted fiber amplifier boosts the signal, which is then sent to a pulse stacker which splits the pulse into multiple different fibers of different lengths and then recombines them into a single fiber so that there is a  $300\text{-ps}$  delay between each of the pulses. The pulse stacker also allows for individual tuning of the energy in each of the pulses. A second fiber amplifier amplifies this pulse stack to make up for the losses incurred in the pulse stacker. At this point, the pulse stack is split into six different fibers so that the seed can ultimately be delivered to up to six different locations in NIF. A third amplifier is used to individually tune the seed energy sent to each of the six locations. The pulse stack then passes through an acousto-optic modulator so that delivery of the seed to the  $4\omega$  airbox may be controlled electronically. Each of the six locations is supported by two pump chassis, in which the pump diodes for the  $4\omega$  airbox fiber amplifier are located. The pulse stack and both pumps are relayed to each of the  $4\omega$  airbox locations via three infrastructure fibers. The pumps are delivered with single-mode (SM) fiber, and the seed is delivered via polarizing (PZ) fiber. See Fig. 2 for a schematic of the facility layout.

With the desired  $1\omega$  output energy determined, we designed a 3-stage fiber amplifier system to achieve the desired final  $1\omega$  energy. This layout is given in Fig. 3. The amplifier system is designed for an input pulse-train energy of a few nanojoules and an output pulse-train energy of up to  $12\mu\text{J}$ . For a six-pulse pulse-train, this would result in  $2\mu\text{J/pulse}$  assuming equal energy in each pulse. The first gain stage is  $25\text{-cm}$  of  $2.8\text{-}\mu\text{m}$  core diameter Yb-doped fiber with an absorption of  $975\text{dB/km}$  at our pump wavelength of  $976\text{-nm}$  and achieves a gain up to  $20\times$  when fully pumped. The second and third stages consist of  $31\text{-}$  and  $36\text{-cm}$ , respectively, of  $6\text{-}\mu\text{m}$  core diameter Yb-doped fiber with an absorption of  $1400\text{dB/m}$  at our pump wavelength with gains of  $\sim 10\times$  when fully pumped.

Referring to Fig. 3, one pump laser is coupled into the first two gain stages with a WDM. Between these two stages is a notch filter that blocks ASE but transmits the pump and seed signals. In this design the first gain stage is completely bleached by the pump, and residual pump light continues to propagate and pump the second stage. After the second stage of amplification we use a bandpass filter to transmit only the signal wavelength at  $1053\text{ nm}$ . In addition, an isolator is used so that back-reflections from the free-space optical portion of the system do not re-enter the first two gain stages which, when propagated back to the pump diodes, could result in damage to the diodes. Another WDM is used to couple a second pump laser into the third gain stage. The end of the third gain fiber is angle cleaved at  $15\text{ degrees}$  and the light from this final gain stage is launched directly into a ball lens that gently focuses the light into the first nonlinear crystal with the desired beam diameter of  $140\mu\text{m}$ . This diameter is verified with a beam profiling camera during construction. Because we are operating near the damage threshold of fused silica it is critical that nothing come into contact with the end of the last gain fiber or else fiber-tip damage will occur when the laser amplifier is turned on.

The fiber amplifier circuit is made entirely from single-mode fiber. Because we desire a particular polarization for optimum frequency conversion, we placed an electronically adjustable polarization controller in the beginning of the circuit where the seed pulse has low energy. We thereby tune the output polarization of the amplifier using this upstream polarization controller. The polarization control is done at this early stage so as to avoid excessive nonlinear propagation effects on the pulse when traversing the pigtail fibers that are needed to couple light into and out of the polarization controller. Because extended lengths of single-mode fiber act as  $\lambda/4$  and  $\lambda/2$  waveplates, the seed pulses that come out of the polarization controller in general would need to be elliptically polarized in order to have a linearly polarized signal at the output of the fiber circuit. This fact is important in



MOR

VISAR LAB

DIM / SPIDER

Figure 2. Schematic showing components from the MOR to the streak camera.

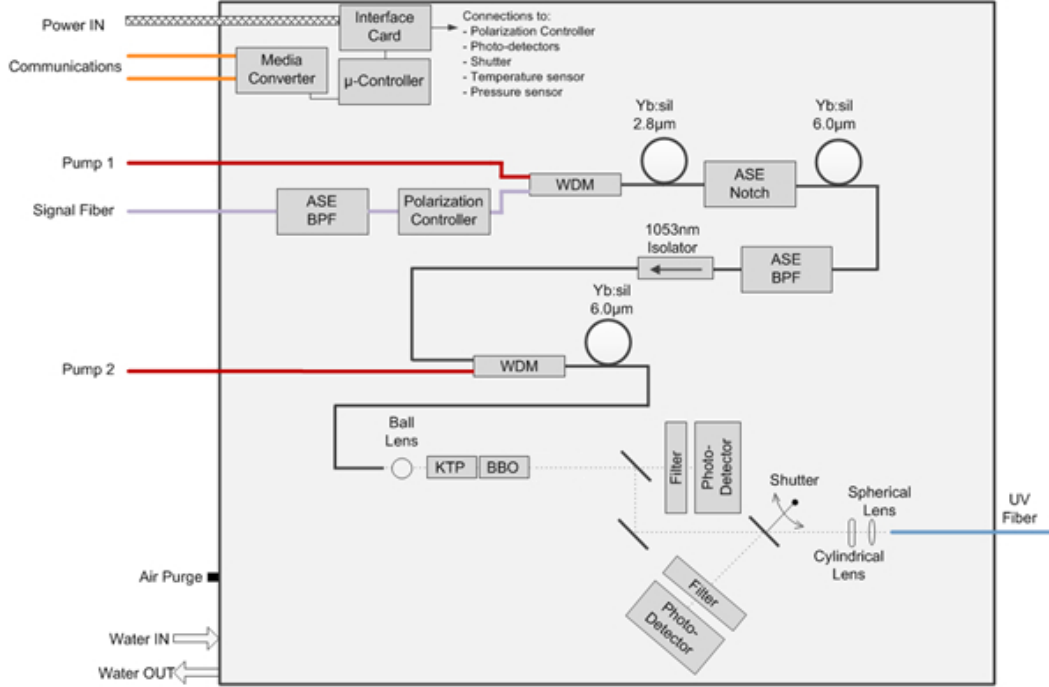


Figure 3. Schematic showing the significant components inside the airbox.

order to understand the performance of the system as pulse energies exceed  $\sim 1\mu\text{J}$  as will be discussed in more detail in Section 3.

The  $2\omega$  signal that comes out of the KTP crystal, in addition to being shortened in time, is also narrowed in space because of the gaussian profile of the  $1\omega$  beam and is  $\sim 100\mu\text{m}$  FWHM, just as required according to the results of the SNLO calculation (see Fig. 1(b)). Therefore the BBO crystal is mounted so that the input to the BBO crystal is right next to the output of the KTP crystal. The  $4\omega$  output from the BBO crystal is elongated because of walk-off between the  $2\omega$  and  $4\omega$  light in the BBO crystal. This asymmetry is corrected with a cylindrical lens before the  $4\omega$  signal is coupled into the  $4\omega$  output fiber that delivers the beam to the streak camera. After the frequency conversion stage, a dichroic mirror is used to reflect the  $4\omega$  light but transmit the  $1\omega$  and  $2\omega$  signals. The  $1\omega$  signal level is monitored with a photodiode and gives us an indication of the health of the amplifier circuit when the airbox is deployed. A shutter can also be placed in the  $4\omega$  beam to block the output of the  $4\omega$  signal. When closed, a mirror on the shutter arm directs the  $4\omega$  signal to a photodiode so that we can determine whether we need to tune the  $1\omega$  polarization to optimize the  $4\omega$  signal. A scaled drawing of the free-space optical path is shown in Fig. 4.

Communication between the airbox and the NIF control system is provided through optical fibers. Inside the airbox an optical-to-electrical converter is used to transmit commands to, and receive data from, a microcontroller device. The microcontroller receives the signals from the  $1\omega$  and  $4\omega$  photodiodes, temperature and pressure monitors within the airbox, and is also used to send commands to the polarization controller. The final size of the airbox is  $160\text{mm}\times 165\text{mm}\times 520\text{mm}$  and fits inside the diagnostic load package behind the DISC or can be attached to the side of the box that houses SPIDER. An air purge line is supplied to correct for small leaks to vacuum, and water lines are used to stabilize the temperature of the airbox.

### 3. PERFORMANCE

The amplifier circuit described above exceeds the specification and can produce  $> 2\mu\text{J}/\text{pulse}$  for a 6-pulse stack. However, we discovered that as per-pulse energies exceed  $1\mu\text{J}$  nonlinear effects begin to negatively affect frequency conversion efficiency and system stability. This is caused by both spectral broadening due to self

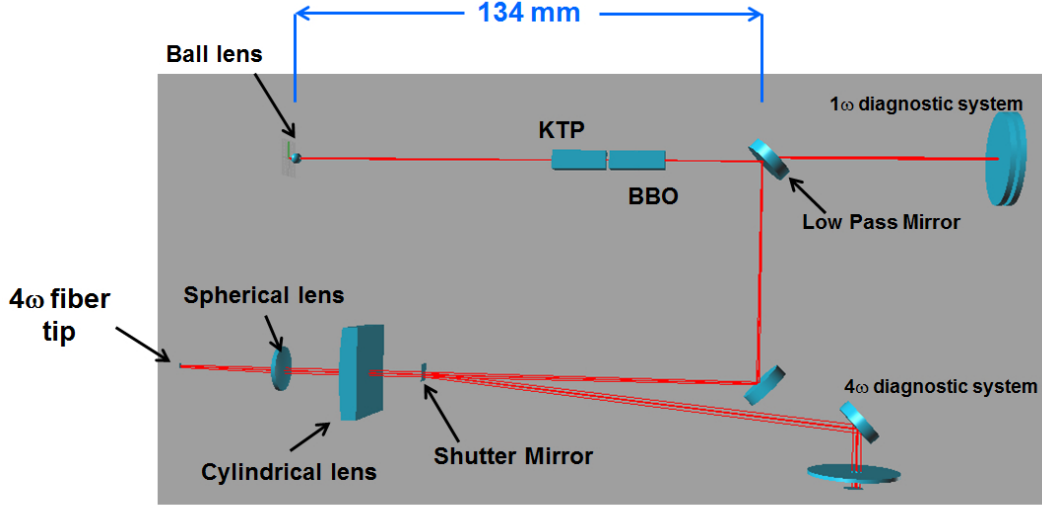


Figure 4. A scaled drawing of the free-space optical path in the  $4\omega$  airbox.

phase modulation (SPM) and nonlinear polarization ellipse rotation. The spectral broadening that results from SPM limits conversion efficiency because the new spectral components do not phase match in the nonlinear crystal as well as the central wavelength for which the system was designed. The SNLO calculations assume a monochromatic source and predicts a higher conversion efficiency than we actually achieve. The spectra for the seed input and 1- and 1.5- $\mu\text{J}$  output pulses are shown in Fig. 5. The spectrum broadens rapidly as the output energy exceeds 1  $\mu\text{J}$ . The nonlinear length,<sup>9</sup>  $L_{NL}$ , which indicates the length over which nonlinear phase modulation becomes significant, is shown in Fig. 6 as a function of pulse energy.  $L_{NL} < 1.5$  cm for a 1- $\mu\text{J}$  pulse. Compare this to the 36-cm length of the final gain fiber. The pulse energy increases approximately exponentially within the fiber, so most of the nonlinear phase is accumulated at the very end of the fiber circuit. To minimize the nonlinear effects we keep the pulse intensities as low as possible in the fiber circuit and maximize the gain in the final stage. We also limit as much as possible the lengths of the multiple fiber pigtailed that are necessary for splicing the different optical components together in the fiber amplifier circuit.

A second nonlinear optical effect to which we are sensitive is nonlinear polarization ellipse rotation.<sup>10</sup> This effect is the rotation of the polarization ellipse as light propagates through a nonlinear medium. If  $\theta$  is the angle that the long axis of the polarization ellipse makes with the ordinate axis, the rotation of that polarization angle is described by

$$\theta = \frac{3\chi_{1221}}{n_0} (|E_-|^2 - |E_+|^2) \frac{\omega}{c} z \quad (1)$$

where  $\chi_{1221}$  is a tensor element of the third-order nonlinear susceptibility,  $E_-$  and  $E_+$  are the left- and right-circularly polarized electric field components, and  $z$  is the propagation distance. The fiber amplifier in the  $4\omega$  airbox has square-pulse distortion, which means the pulses at the end of the pulse train experience less gain than those at the beginning. This occurs as the gain is extracted by the leading-edge pulses and gain medium is no longer saturated as the subsequent pulses propagate through the gain region. This means that the pulse stack that is injected at the beginning of the amplifier circuit must be ramped, as shown in Fig. 7(a) so that the output pulses have approximately equal energies as shown in Fig. 7(b). However, if the output pulses are passed through a polarizing optic, in this case a polarizing fiber, we see that each pulse has a different polarization as shown in Fig. 7(c). This occurs because the nonlinear polarization ellipse rotates to a different angle for each pulse because of their different intensities in the amplifier circuit. Because nonlinear frequency conversion is sensitive to polarization angle, even though the six pulses all have the same  $1\omega$  energy, the  $2\omega$  pulse train has six pulses with different amounts of energy. The  $2\omega$  pulse train is well-polarized because of the nature of the second-harmonic generation, but the  $2\omega$  variation in pulse energies is amplified when the pulse train is converted to  $4\omega$

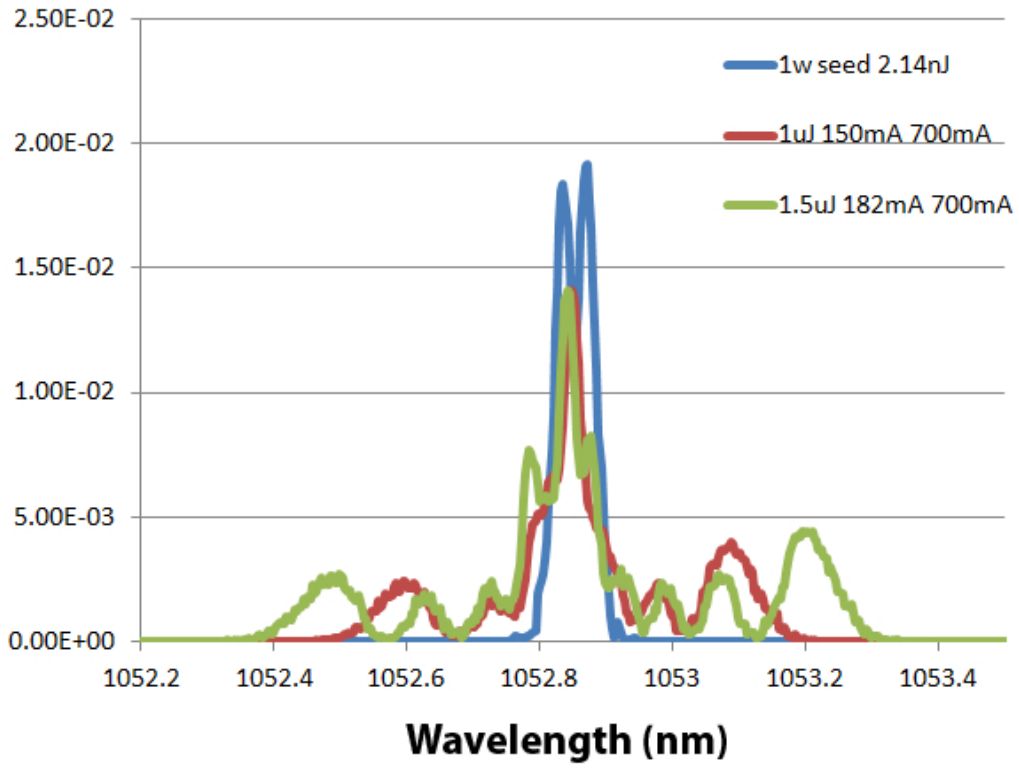


Figure 5. Spectrum of the seed pulse at the input to the amplifier (blue), with  $1\mu\text{J}/\text{pulse}$  (red) and  $1.5\mu\text{J}/\text{pulse}$  of output power (green).

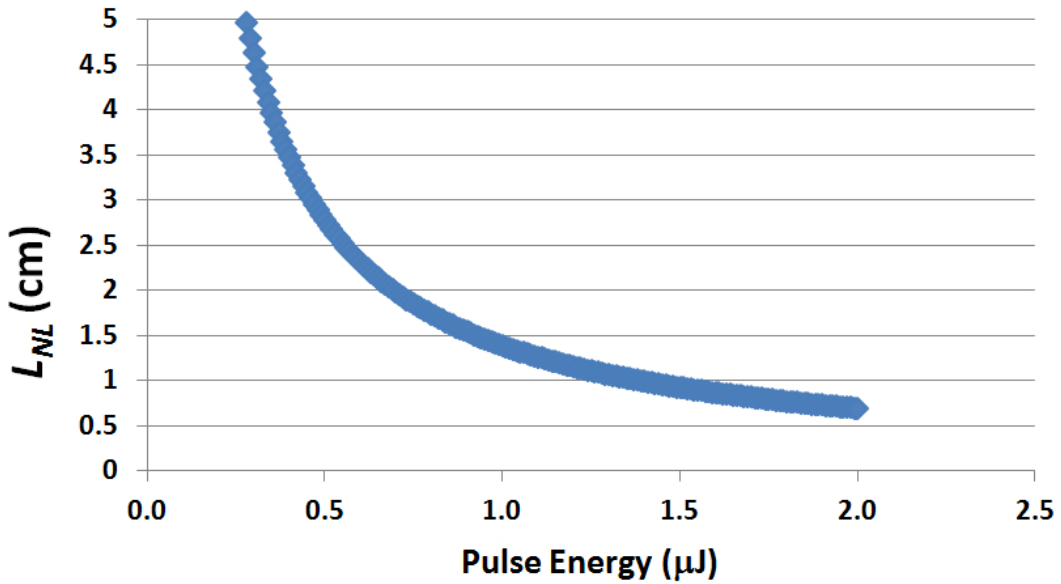


Figure 6. Nonlinear length  $L_{NL}$  vs. pulse energy.

because of the nonlinear nature of the frequency conversion process. Furthermore, this process is very sensitive to environmental conditions, so small changes in fiber temperature, for example, can lead to large shot-to-shot variations in the  $4\omega$  pulse train. For this reason we pursued two paths to improve system stability: we turned down the  $1\omega$  energy output from the fiber amplifier from  $2\ \mu\text{J}$  to  $1\ \mu\text{J}/\text{pulse}$ , and we reduced the number of pulses from six to three by fully attenuating every other pulse at the pulse stacker. Lowering the output energy lowers the nonlinear phase shift and improves the output spectrum. Going from six pulses to three reduces the amount of square-pulse distortion and helps to minimize the effects of nonlinear polarization rotation by ensuring the pulses in the input pulse train are launched with closer to the same intensity.

Because we desired to reduce the required  $4\omega$  energy per pulse, we undertook a photocathode study in which we tested several different photocathodes to determine which material generated the most photoelectrons when exposed to  $4\omega$  light. We tested gold, silver, titanium, and several different thicknesses of aluminum. We found aluminum was most sensitive to the  $4\omega$  signal and this is the material we have used for testing and will use for the deployed system. For aluminum, the required  $4\omega$  energy per pulse is  $1\ \text{nJ}$  at the photocathode. The details of this study can be found in Ref. 11. Using aluminum for a photocathode has allowed us to have greater margin on the  $4\omega$  energy, and we typically get up to  $28\ \text{nJ}/\text{pulse}$  of  $4\omega$  light out of the  $4\omega$  airbox. When the coupling and transmission losses through the streak camera hardware are accounted for, we estimate that we can get up to  $7\ \text{nJ}/\text{pulse}$  onto the photocathode which is  $7\times$  the energy requirement for an aluminum photocathode.

An example of a typical spot image on the X-ray streak camera for a three-pulse fiducial is shown in Fig. 8. The streak camera image shows three spots on the the left hand side of the image. The time axis is vertical and the space axis is horizontal. The fiducial spacing is  $600\ \text{ps}$  between pulses and the streak camera has a  $3\text{-ns}$  window. The results of a study of streak camera signal vs.  $4\omega$  pulse energy are shown in Fig. 9. Figure 9(a) shows the average signal level in a  $250\times 250$ -pixel region of interest (ROI) around the peak of each pulse, and Fig. 9(b) shows the peak-pixel signal for each of the spots. On these graphs  $1500\text{mV}$  corresponds to  $7\ \text{nJ}$  of  $4\omega$  at the photocathode and the relationship between  $4\omega$  detector voltage and energy is linear. One can see that as the  $4\omega$  pulse energy is decreased (by decreasing the  $1\omega$  seed energy) the spread in signal on the photocathode decreases. This is because the nonlinear effects discussed above have less of an impact on the frequency conversion, and thus the  $4\omega$  output signal is more stable. Figure 9(b) shows that even at  $\sim 2\ \text{nJ}/\text{pulse}$ , sufficient fiducial signal exists. It should be noted that the absolute lower limit of  $4\omega$  energy varies from photocathode to photocathode and is also strongly affected by the geometry of the wire grid that is used to accelerate the electrons down the streak tube. Work to improve this geometry is currently underway. This wire grid can be seen in Fig. 10, which is a close-up mechanical drawing of the photocathode, associated electronics, and the fiber by which the  $4\omega$  signal is delivered to the photocathode.

## 4. CONCLUSION

While the system design presented here meets the current requirements, there are several improvements we plan to make. First, we intend to return to six-pulse operation instead of three-pulse operation. Initial modeling has shown that improving the photocathode grid geometry can greatly increase the signal level from the fiducial coming from the photocathode. This would further lower the required  $4\omega$  signal and allow us to operate in a regime in which the nonlinear polarization rotation is not as drastic, so that square-pulse distortion would not lead to the same level instability we see at the current  $1\omega$  energy levels. A second potential improvement to the system involves using polarization maintaining (PM) fiber in the  $4\omega$  airbox amplifier circuit instead of the SM fiber that is currently being used. This would allow us to increase the  $1\omega$  output signal without losing conversion efficiency due to nonlinear polarization rotation.

## REFERENCES

- [1] Kimbrough, J. R., Bell, P. M., Bradley, D. K., Holder, J. P., Kalantar, D. K., MacPhee, A. G., and Telford, S., "Standard deisgn for NIF X-ray streak and framing cameras," *Rev. Sci. Instrum.* **81**, 10E530 (2010).
- [2] Hicks, D. G., Spears, B. K., Braun, D. G., Olson, R. E., Sorce, C. M., Celliers, P. M., Collins, G. W., and Landen, O. L., "Streaked radiography measurements of convergent ablator performance," *Rev. Sci. Instrum.* **81**, 10E304 (2010).

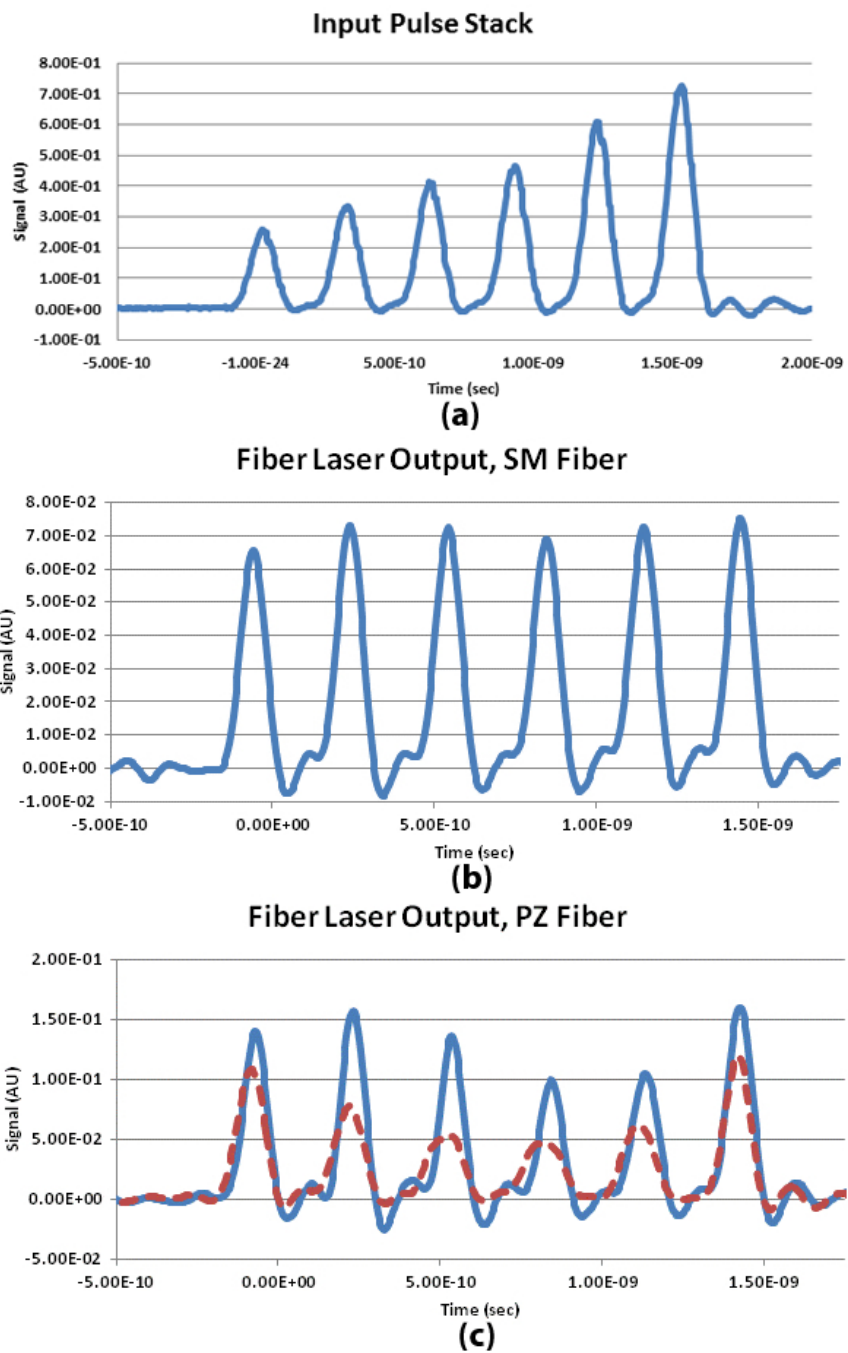


Figure 7. Measured pulse-stack for: (a) the input to the amplifier, (b) as measured at the output of the amplifier, and (c) as measured at the output of the amplifier after coupling into a polarizing (PZ) fiber.

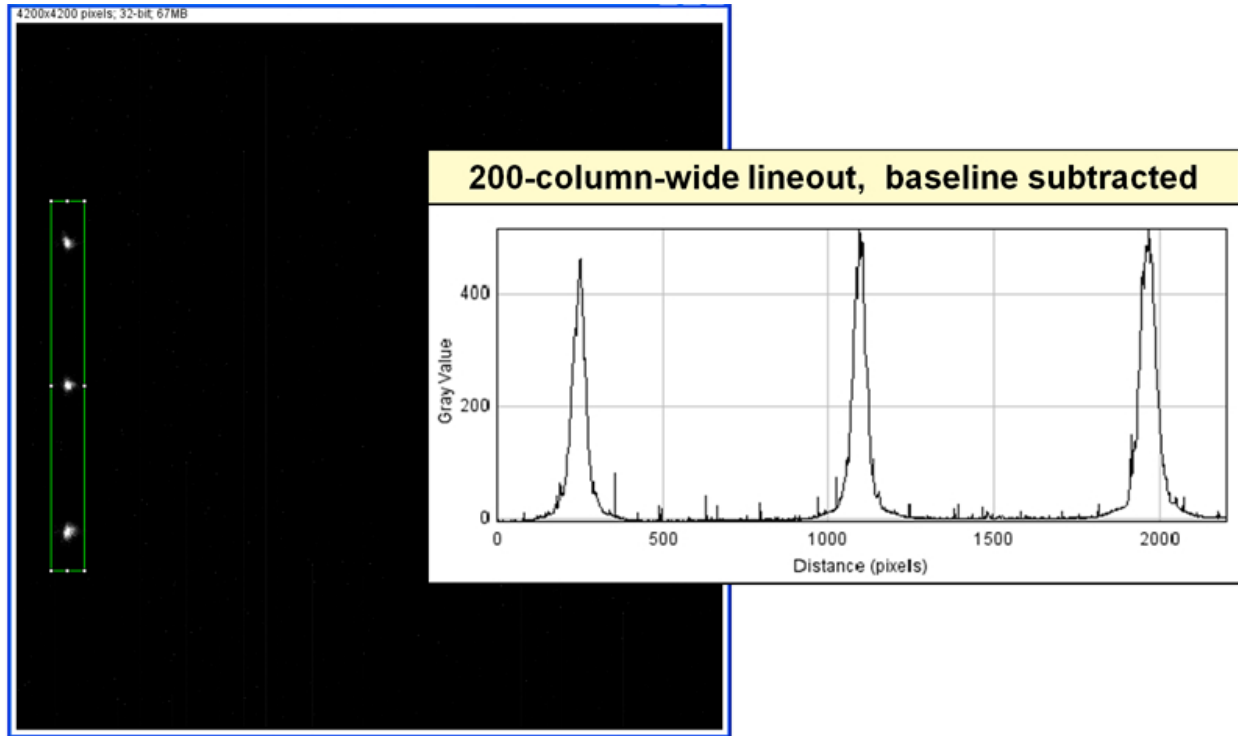


Figure 8. Streak camera data and a line-out of a 200-column-wide box after baseline subtraction.

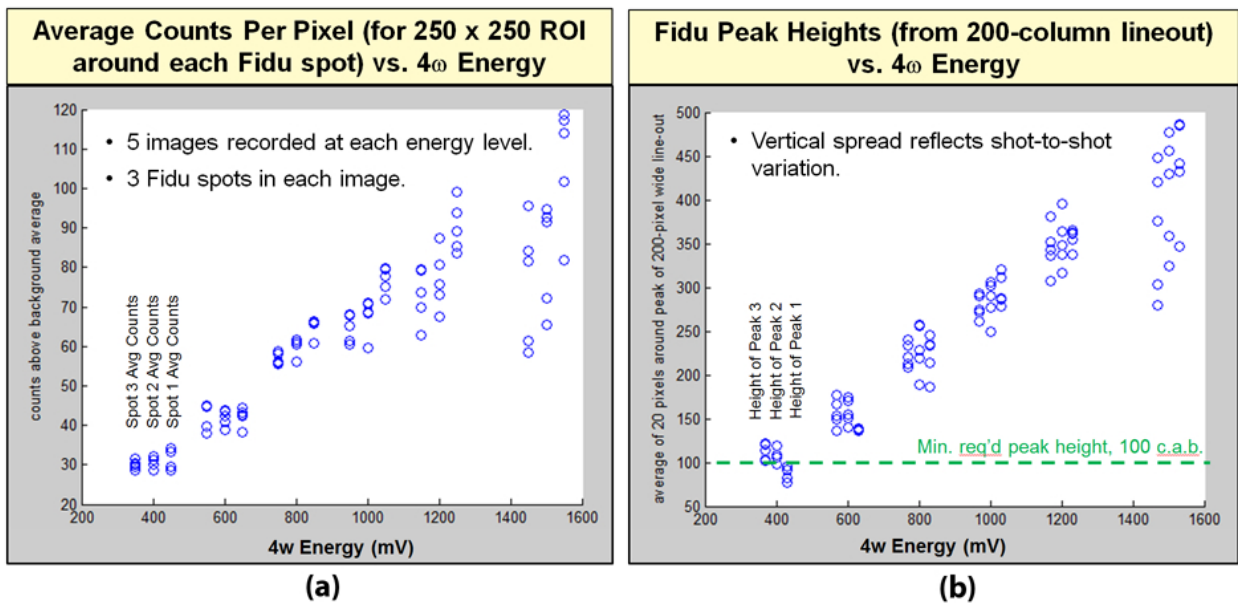


Figure 9. Streak camera spot signal versus  $4\omega$  pulse energy indicating the average signal of each of the three spots (a) and the peak signal in each of the three spots (b). The  $4\omega$  signal in millivolts can be converted to nJ by multiplying the millivolt value by 0.0187.

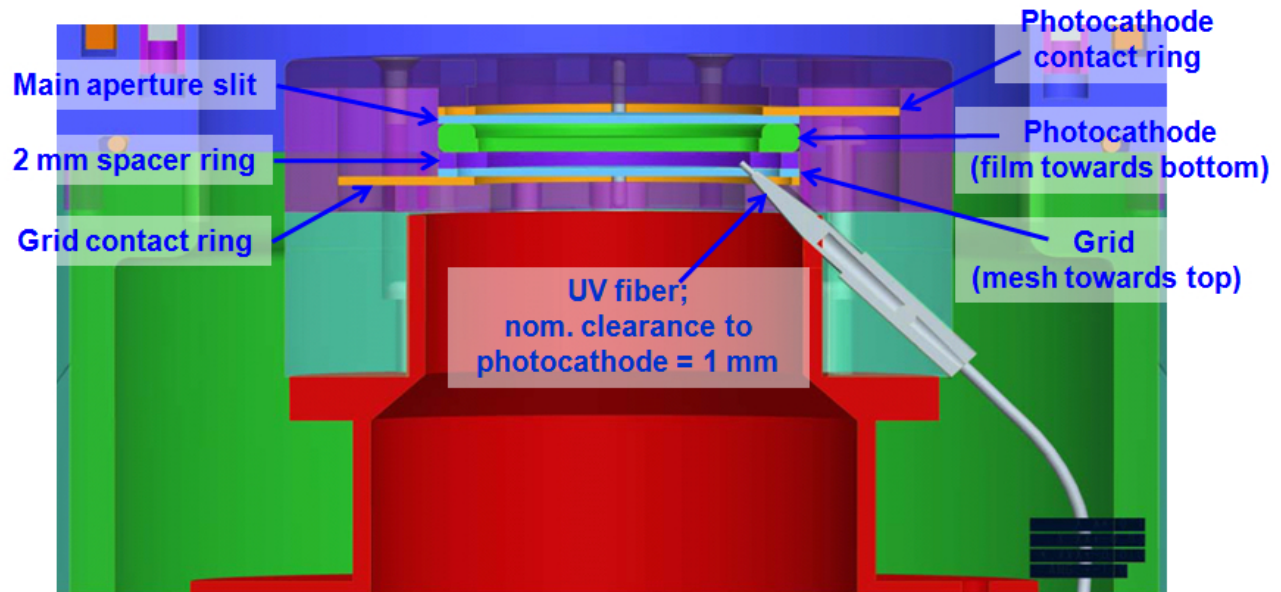


Figure 10. UV photocathode design in DISC and the UV delivery fiber. The X-ray signal comes from the top, while the  $4\omega$  fiducial illuminates the backside of the photocathode.

- [3] Khan, S. F. and Celeste, J. R., “Measuring x-ray burn history with the Streaked Polar Instrumentation for Diagnosing Energetic Radiation (SPIDER) in the National Ignition Facility (NIF),” *Proc. SPIE* **8505**, 8505–4 (2012).
- [4] Michael R. Charest, J., Torres, P., III, Silbernagel, C. T., and Kalantar, D. H., “Reliable and repeatable characterization of optical streak cameras,” *Rev. Sci Instrum.* **79**(10), 10F546 (2008).
- [5] Okishev, A. V. and Zuegel, J. D., “Highly stable, all-solid-state nd:y:lf regenerative amplifier,” *Appl. Opt.* **43**, 6180–6186 (Nov 2004).
- [6] Available free from <http://www.as-photonics.com/snlo>.
- [7] Stuart, B. C., Feit, M. D., Rubenchik, A. M., Shore, B. W., and Perry, M. D., “Laser-induced damage in dielectrics with nanosecond to subpicosecond pulses,” *Phys. Rev. Lett.* **74**, 2248–2251 (Mar 1995).
- [8] Wisoff, P. J., Bowers, M. W., Erbert, G. V., Browning, D. F., and Jedlovec, D. R., “NIF injection laser system,” *Optical Engineering at the Lawrence Livermore National Laboratory II: The National Ignition Facility* **5341**(1), 146–155, SPIE (2004).
- [9] Agrawal, G. P., [*Nonlinear Fiber Optics*], Academic Press (1995 (2nd edition)).
- [10] Boyd, R. W., [*Nonlinear Optics*], Academic Press, San Diego (2008 (3rd edition)).
- [11] Opachich, Y., Palmer, N., Homoelle, D., Hatch, B., Bell, P., Bradley, D., Kalantar, D., Browning, D., Zuegel, J., and Landen, O., “X-ray streak camera cathode development and timing accuracy of the  $4\omega$  ultraviolet fiducial system at the national ignition facility,” *Rev. Sci. Instrum.* **83**, 10E123–1 (2012).